Differences in Secondary Structure between Packaged and Unpackaged Single-Stranded DNA of Bacteriophage ϕX174 Determined by Raman Spectroscopy: A Model for ϕX174 DNA Packaging†

James M. Benevides,‡ Patricia L. Stow,§ Leodevico L. Ilag,§ Nino L. Incardona,§ and George J. Thomas, Jr.*,‡

Division of Cell Biology and Biophysics, School of Basic Life Sciences, University of Missouri—Kansas City, Kansas City, Missouri 64110-2499, and Department of Microbiology and Immunology, University of Tennessee—Memphis, Memphis, Tennessee 38163

Received June 8, 1990; Revised Manuscript Received January 31, 1991

ABSTRACT: The single-stranded packaged genome (ssDNA) of bacteriophage ϕX174 is shown by Raman spectroscopy to lack both the ordered phosphodiester backbone and base stacking, which are demonstrated for unpackaged, protein-free ssDNA. In solutions of moderate ionic strength, *unpackaged* ssDNA contains 36 ± 7% of deoxyribosyl phosphate groups with conventional B-type backbone geometry [i.e., gauche$^-$ and trans orientations, respectively, for the 5′O–P (α) and 3′O–P (ζ) torsions], indicative of hairpin formation and intramolecular base pairing. Additionally, the bases of unpackaged ssDNA are extensively stacked. Estimates from Raman band hypochromic effects indicate that unpackaged ssDNA contains approximately 70% of the maximal base stacking exhibited in the linear, double-stranded, replicative form III of ϕX174 DNA. Conversely, for the packaged ϕX174 genome, ordered (B-type) phosphodiester groups are not present, and only 40% of the base stacking in RFIII DNA is observed. These results are interpreted as evidence that the substantial hairpin-forming potential of ssDNA is eliminated by specific and extensive ssDNA–protein interactions within the ϕX174 virion. Comparison of the present results with studies of other packaged single-stranded nucleic acids suggests that proteins of the capsid shell (gpF + gpG + gpH) do not fully account for the conformational constraints imposed on ssDNA of ϕX174. Accordingly, we propose a model for ssDNA packaging in which the small basic gpJ protein, which is packaged along with the genome, is involved stoichiometrically in binding to the ssDNA (≈90 nucleotides per subunit). The proposed gpJ–DNA interactions could prevent helical hairpin formation, restrict base stacking, and disfavor fortuitous base pairing within the capsid. The present analysis is based upon use of model nucleic acids of known conformation for calibration of the Raman intensity in the region 810–860 cm^{-1} in terms of specific secondary structures. The calibration curve allows quantitative determination of the percentage of ssDNA nucleotides for which the 5′O–P–O3′ group is configured (g$^-$,t) as in the B-form of DNA. The method proposed here is analogous to that employed by Thomas and Hartman (1973) for ssRNA and should be applicable to single-stranded DNA and to partially denatured forms of double- and multiple-stranded DNAs.

ϕX174 is a small icosahedral bacteriophage which packages a circular single-stranded DNA molecule of 5386 nucleotides encoding 11 gene products (Sanger et al., 1978; Shaw et al., 1978; Hayashi et al., 1988). The viral capsid consists of 60 copies each of proteins gpF (48.40 kDa) and gpG (19.05 kD) and 12 copies of protein gpH (34.40 kDa). The mature virion also packages 60 copies of a highly basic protein, gpJ (4.10 kDa) (Burgess, 1969; Siden & Hayashi, 1974). Although molecular biological studies of ϕX174 have provided important insights into mechanisms of prokaryotic gene replication (Kornberg, 1980), relatively little is known of the detailed structure and macromolecular organization of the virion.

Investigation of the ϕX174 crystal structure by X-ray and electron diffraction methods is in progress (N. Incardona and M. G. Rossman, unpublished results) and should lead to a more detailed understanding of the capsid architecture. Initial results indicate a monoclinic unit cell of space group $P2_1$ containing two phage particles of diameter 280 Å (Willingmann et al., 1990). Since the preliminary diffraction data also show that particles which package complete and incomplete genomes have the same capsid morphology, it is not likely that the electron density map can fully reveal the location of ssDNA in the mature virion. The conformation of the packaged ssDNA circle and its interactions with capsid peptides (surface and/or interior) require investigation by other biochemical and biophysical methods. The small size and relative simplicity of the ϕX174 virion, as well as the known sequences of phage protein and nucleic acid constituents, are factors favorable to its study by Raman spectroscopy (Thomas, 1987). Methods of Raman spectroscopy should be particularly effective in identifying secondary structures of the packaged ssDNA and possible DNA–protein interactions in the virion.

In a recent Raman study of ϕX174 phage particles, Incardona et al. (1987) demonstrated β-sheet secondary structures of capsid proteins and probed the packaged ssDNA conformation. In the previous work, neither isolated capsid proteins (free of DNA) nor purified protein-free ssDNA was available in quantity sufficient for direct Raman examination. Accordingly, the Raman signature of ϕX174 ssDNA was deduced by Fourier deconvolution of the phage spectrum to eliminate the substantial Raman contributions of capsid proteins, which constitute about 75% of the virion mass. The Fourier analysis facilitated interpretation of ssDNA Raman bands in the phage spectrum and revealed that the packaged

† This is part 30 in the series "Studies of Virus Structure by Laser Raman Spectroscopy" and is supported by NIH Grant AI11855 (G.J.T.) and NSF Grant DMB-8416573 (N.L.I.).

* To whom correspondence should be addressed.

‡ University of Missouri—Kansas City.

§ University of Tennessee—Memphis.

0006-2960/91/0430-4855$02.50/0 © 1991 American Chemical Society

genome contained little, if any (<15%), base-paired secondary structure. Incardona et al. (1987) showed further that the Raman signature of packaged ssDNA resembled that of heat-denatured DNA, which lacks bands diagnostic of a regularly ordered phosphodiester backbone. Since single-stranded nucleic acids in solution typically form stable hairpins containing substantial numbers of paired bases with a regularly ordered sugar–phosphate backbone, it was suggested that constraints imposed by the viral proteins probably restrict helical hairpin formation and base pairing in the packaged state of ϕX174 DNA (Incardona et al., 1987).

Protein-free ssDNA has now been isolated from ϕX174 in sufficient quantity and purity for Raman spectroscopy. We have also isolated in a highly purified state the corresponding double-stranded supercoiled DNA (replicative form I, or RFI DNA) following ϕX174 infection of *Escherichia coli*. In the present paper we compare the Raman signatures of packaged and protein-free ssDNA with spectra of the linearized or RFIII form of the dsDNA. These data are compared with corresponding spectra of model single-stranded and double-stranded oligonucleotides, and with spectra obtained from a DNA-depleted ϕX174 capsid (low density 70S component; Willingmann et al., 1990). The results are interpreted to provide quantitative estimates of the degree of order in the DNA backbone and the extent of base-stacked secondary structures of ssDNA in packaged and unpackaged states of ϕX174, and additionally to identify conformational constraints imposed on ssDNA by phage packaging.

Raman spectroscopy has been employed previously to assess phosphodiester and nucleoside conformations in *double-stranded* nucleic acids, including RNA and DNA (Lafleur et al., 1972; Brown et al., 1972; Thomas & Hartman, 1973; Erfurth et al., 1975; Thamann et al., 1981; Prescott et al., 1984; Thomas et al., 1986a; Benevides et al., 1986, 1988). In a review of applications to DNA crystals of known three-dimensional structures (Thomas & Wang, 1988), the conformation-sensitive bands and their correlated nucleoside and phosphodiester conformations have been tabulated. In the present study, we extend the previously developed Raman spectra/structure correlations to include *single-stranded* DNA. We show that Raman intensities which originate from vibrations of the phosphodiester backbone may be exploited for quantitative determination of the degree of ordered B-form secondary structure that is contributed by helical hairpins and tertiary interactions of packaged ssDNA. The method developed here should be applicable to other ssDNA molecules and should also have value for characterizing unpaired domains of double-stranded and multiple-stranded DNAs.

Materials and Methods

(1) Preparation of Bacteriophage. Raman spectra of the intact phage and low-density 70S component were obtained on samples of the lysis-defective mutant E*am*3. The conditions for growth and purification were the same as described in Incardona et al. (1987) with the following modifications. The pooled sucrose gradient fractions containing the 70S component were concentrated by differential centrifugation after the sucrose was removed by dialysis against borate buffer containing 0.1 M NaCl. The sample was then centrifuged through a second sucrose gradient. The pooled fractions from this gradient were then dialyzed against borate buffer, and dry CsCl was added to give a final density of 1.34 g/mL for the isopycnic centrifugation. Only fractions on the low-density side of the broad peak were pooled to ensure that the preparation contained particles with the least amount of DNA. Both Raman and UV spectra show that more than 85% of the normally packaged genome is absent from these low-density 70S particles.

(2) Isolation and Purification of ϕX174 DNA. Circular ssDNA was isolated from E*am*3 phage purified by differential centrifugation. Crude lysates, prepared as described by Incardona et al. (1987), were centrifuged at 30000 rpm for 2 h at 5 °C in the Beckman 42.1 rotor. The pellets were resuspended in pH 9.0 borate buffer (sodium tetraborate saturated at 5 °C) and subjected to low-speed centrifugation for 10 min in an Eppendorf 5412 centrifuge at room temperature to remove any insoluble debris. After a second cycle of high- and low-speed centrifugation, the phage preparation contained little or no host DNA as judged by the A_{260}/A_{280} optical density ratio. The phage sample was mixed vigorously with an equal volume of borate buffer saturated phenol (55 °C), incubated with intermittent shaking at 55 °C for 15 min, and the two phases were separated by a 10-min spin at 5000 rpm in a clinical centrifuge at room temperature. The clear aqueous phase was then dialyzed against 10 mM Tris-HCl and 0.1 M NaCl, pH 7.5, to remove the phenol. Two volumes of cold 95% ethanol was added, the samples were placed at −20 °C overnight, and the precipitated DNA was collected by centrifugation. The pellets were resuspended in 10 mM Tris-HCl and 1 mM EDTA, pH 8.0 (TE) and aliquots were analyzed by agarose gel electrophoresis and electron microscopy. No additional ethidium bromide staining bands were observed, and 90% of the molecules were circular. The DNA was ethanol precipitated and redissolved in the appropriate buffer for Raman spectroscopy.

For purification of RFI DNA a 1200-mL culture of *E. coli* C was grown at 37 °C in TYE medium (Incardona et al., 1985) supplemented with 13 mM $CaCl_2$ to a cell density of 1.0×10^9. After a second addition of the same amount of $CaCl_2$, the culture was infected with ϕX174 E*am*3 at an MOI of 5 and incubated at 37 °C for an additional 10 min. Chloramphenicol was then added to a final concentration of 150 μg/mL. The culture was incubated for an additional 4 h at the same temperature and then stored overnight at 4 °C.

The infected cells were collected by centrifugation and lysed by a modified Birnboim and Doly procedure (Birnboim & Doly, 1979). The cell pellets were resuspended in 120 mL of solution 1 (59 mM glucose, 10 mM EDTA, 25 mM Tris, pH 8.0); 120 mg of hen egg white lysozyme was added, and the suspension was mixed vigorously. The suspension was kept on ice for 10 min before 140 mL of solution 2 (0.2 N NaOH, 1% SDS) was added and the suspension was mixed by inversion. After an additional 10 min on ice 180 mL of solution 3 (3 M $KC_2H_3O_2$, 1.8 M formic acid) was added and the suspension was mixed by inversion until a flocculent precipitate formed. This mixture was kept on ice for 15 min before the precipitate was removed by centrifugation at 4 °C. The supernatant containing the covalently closed, double-stranded, superhelical ϕX174 RFI DNA was saved.

One liter of cold 95% ethanol was added to the RFI DNA solution, and the mixture was then kept at −20 °C for at least 6 h to allow precipitation of the DNA. The DNA pellet was collected by centrifugation and resuspended in 2.0 mL of TE (10 mM Tris-HCl, 1 mM EDTA, pH 8.0). The RFI DNA was further purified by equilibrium centrifugation in a CsCl–ethidium bromide gradient (initial density 1.55 g/mL, ethidium concentration 250 μg/mL) in a Beckman VTi50 rotor at 45000 rpm for 15 h at 15 °C. The RFI band was collected from the side of the tube with a hypodermic needle, and the ethidium bromide was removed by several extractions with CsCl-saturated 2-propanol. The DNA was separated

from the CsCl by four consecutive precipitations with ethanol. Total yield was 11.03 mg, and the A_{260}/A_{280} ratio was 1.90. The homogeneity was also checked by agarose gel electrophoresis.

(3) *Preparation of φX174 RFIII DNA.* Five milliters of φX174 RFI DNA (0.86 mg/mL) in TE was mixed with 1.0 mL of 10× restriction digest buffer (1× = 50 mM Tris-HCl, 10 mM $MgCl_2$, 75 mM NaCl, 1 mM DTT, pH 7.5), 14.0 mL of sterile distilled water, and 80 μL of restriction enzyme *PstI* (20 units/μL, New England Biolabs). After a 1-h digestion at 37 °C, 40 mL of cold 95% ethanol was added and the sample was kept at −20 °C for 6 h. Complete digestion (>97%) was verified by agarose gel electrophoresis and electron microscopy. The precipitated DNA was collected by centrifugation in the Sorvall GSA rotor at 10000 rpm for 10 min at 4 °C and resuspended in 4.0 mL of TE buffer. The sample was then extracted with an equal volume of TE-saturated phenol, followed by dialysis of the aqueous layer against TE buffer plus 0.15 M NaCl. The RFIII DNA was ethanol precipitated and the dry pellet redissolved as required for Raman spectroscopic analysis.

Since ssDNA of φX174 contains unequal proportions of the bases (23.95% A, 31.27% T, 23.30% G, 21.48% C), RFIII DNA differs slightly from ssDNA in total base composition (3.7% more A, 3.7% less T, 0.9% less G, and 0.9% more C) (Kornberg, 1980). These differences in primary structure are relatively small and are easily compensated when comparing the spectra of ssDNA and RFIII DNA. The Raman spectrum of RFIII is thus conveniently employed as a control to represent the Raman signature of a hypothetical B-form (completely base-paired) viral genome.

(4) *DNA Oligomers.* In addition to RFIII dsDNA, we have employed synthetic DNA oligomers as model compounds for fully base-paired dsDNA. Nonadecamer strands of d(ATACCACTGGCGGTGATAT)·d(ATATCACCGCCAGTGGTAT), which contain the phage λ O_L1 operator sequence, were synthesized and purified at the DNA Synthesis Service, Department of Chemistry, University of Pennsylvania, Philadelphia, PA 19104. The strands were combined in equimolar proportions as determined from UV absorbance measurements and annealed at 50 °C, followed by slow cooling. The solution of the 19-mer duplex was lyophilized to near dryness and redissolved at the concentration required for Raman spectroscopy, as next described. The nonadecamer single strand d(ATACCACTGGCGGTGATAT) (hereafter O_L1+) was examined at elevated temperature as a model for ssDNA.

(5) *Raman Spectroscopy.* Solutions (≈40 mg/mL) of phage φX174, ssDNA, RFIII DNA, O_L1, and O_L1+ were prepared for Raman analysis by dissolving the appropriate nucleic acid in an aqueous solution containing 100–200 mM NaCl, adjusted to pH 7.4 ± 0.1 with dilute NaOH. Solutions were sealed in Raman capillary cells (Kimax 34507) and thermostated at 12 °C during recording of Raman spectra. The spectra were excited with 150–200 mW of 514.5-nm radiation from a Coherent Innova Model 70 argon laser and were recorded on a Spex Ramalog V/VI spectrometer under the control of an IBM-XT microcomputer. Programs for the recording and manipulation of spectral data on the IBM-XT were developed in our laboratory with the ASYST system software (ASYST Technologies). Raman spectra displayed in the figures are the averages of 5 or more scans, of 1.5 cm^{-1} or better repeatability. Each scan was obtained at an interval of 1.0 cm^{-1} with an integration time of 1.5 s. A spectral slit width of 8 cm^{-1} was employed throughout. In each case, scattering by solvent was removed by using computer subtraction techniques described previously (Benevides et al., 1984). Raman frequencies are accurate to within ±2 cm^{-1}.

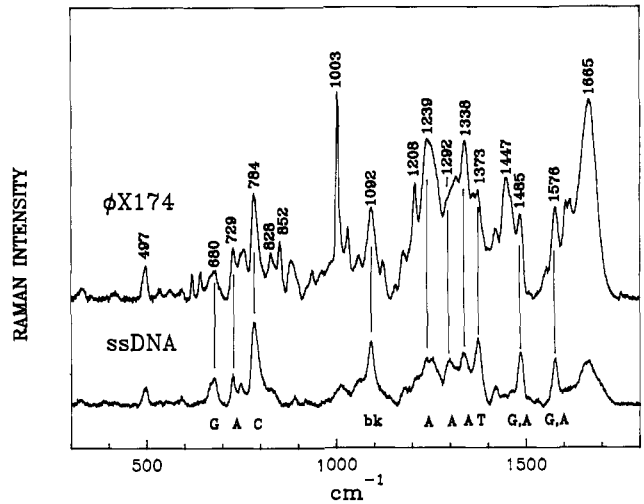

FIGURE 1: Raman spectra in the region 300–1800 cm^{-1} of bacteriophage φX174 (50 mg/mL; top) and protein-free ssDNA (25 mg/mL; bottom), each at pH 7 and 12 °C. Labels indicate Raman frequencies in cm^{-1} units and base residue (A, C, G, T) and backbone (bk) assignments. The ssDNA spectrum was scaled to yield the same apparent intensities for corresponding DNA bands of the phage (vertical lines). Both spectra were corrected for solvent. Complete band assignments are given by Incardona et al. (1987).

Software for curve decomposition by Fourier deconvolution has been described (Thomas & Agard, 1984). The deconvolution procedure conserves intensities of the deconvoluted bands as well as the band envelope. A Gaussian–Lorentzian product function of 18 cm^{-1} half-width was used as the desmearing function for deconvolution. To reduce spectral noise, data were smoothed with a 13-point convolution smoothing routine before deconvoluting. In no instance did the smoothing significantly change either the Raman line frequencies or intensities. Band area measurements were facilitated by commercially available software applications for IBM microcomputers (Instruments SA, Edison, NJ).

RESULTS

(1) *Raman Spectra of ssDNA in Packaged and Unpackaged States.* Figure 1 (top) shows the Raman spectrum of phage φX174 in the region 300–1800 cm^{-1}. The protein bands, which dominate this spectrum, are the composite of gpF (60 subunits), gpG (60), gpH (12), and gpJ (60), accounting for 61.6%, 24.3%, 8.8%, and 5.3% of the phage protein, respectively. The DNA bands are those of the packaged, single-stranded, circular ssDNA molecule, which constitutes about 27% of the virion mass. The Raman bands of DNA and protein in the phage spectrum of Figure 1 are consistent with those reported previously (Incardona et al., 1987) and exhibit markedly improved spectral resolution and signal intensity.

Figure 1 (bottom) shows the Raman spectrum of φX174 DNA isolated from the phage by phenol extraction. All bands in this spectrum are those of the unpackaged ssDNA, allowing identification of Raman bands of the phage that arise from the packaged ssDNA. For evaluation of secondary structure of packaged ssDNA, we examined Raman bands of the interval 600–900 cm^{-1}. This fingerprint region contains two types of DNA conformation indicators: (i) *nucleoside markers*, which identify sugar pucker and glycosyl torsion, and (ii) *backbone markers*, which are characteristic of torsions ($\alpha,\beta,\gamma,\delta,\epsilon,\zeta$) of the P–O5′–C5′–C4′–C3′–O3′–P backbone (Thomas et al., 1986a). An abbreviated listing of DNA

Table I: Conformation Markers in Raman Spectra of A-, B-, and Z-DNA[a]

residue	B-DNA	A-DNA	Z-DNA
G	682 ± 2	664 ± 2	625 ± 3
	1318 ± 2	1333 ± 3[b]	1316 ± 2
A	663 ± 2	644 ± 4	624 ± 3
	1339 ± 2	1335 ± 2	1310 ± 5
C	782 ± 2	780 ± 2	784 ± 2
	1255 ± 5	1252 ± 2	1265 ± 2
T	748 ± 2	745 ± 2	
	790 ± 3	777 ± 2	
	1208 ± 2	1239 ± 2	
backbone	790 ± 5	705 ± 2	745 ± 3
	835 ± 7[c]	807 ± 3[d]	
	1092 ± 1	1099 ± 1	1095 ± 2
	1422 ± 2	1418 ± 2	1425 ± 2

[a] Frequencies in cm^{-1} units are determined from Raman spectra of DNA crystals and fibers of known structure. See Thomas and Wang (1988) and references cited therein. [b] A weak companion line near 1316 cm^{-1} is also observed in B-DNA structures. [c] The position of this line is sensitive to base composition as discussed in text. [d] This line occurs at 813 ± 3 cm^{-1} in A-RNA structures. In Z-DNA structures a weak line is present near 810 cm^{-1}.

conformation markers is given in Table I. More detailed discussion can be found in recent reviews (Nishimura & Tsuboi, 1986; Thomas & Wang, 1988).

In order to interpret the Raman markers of packaged ssDNA, the interfering bands of the phage proteins must be compensated in the phage spectrum. Direct and complete subtraction of all capsid proteins has been employed for cases in which viral morphogenesis can be controlled to yield pure empty capsids (Thomas et al., 1982; Verduin et al., 1984; Li et al., 1990). Since compensation by direct digital subtraction of spectral contributions from all phage proteins is more problematic for ϕX174 (see section 3b, below), we have employed as a first approximation a method based upon Fourier deconvolution (Thomas & Agard, 1984; Incardona et al., 1987). In this procedure the spectrum of the phage is deconvoluted to separate protein and DNA Raman bands. The deconvoluted protein bands are then subtracted, and the remaining DNA bands are reconvoluted with the original deblurring function to regenerate the Raman profile corresponding to the packaged ssDNA. Since band intensities are conserved at each step of this process, quantitative separation of partially overlapped bands is straightforward (Thomas & Agard, 1984). In the case of two extensively overlapped bands, quantitative determination of one is possible if the intensity of the other is reliably known. This is the case for the composite 828-cm^{-1} band of phage ϕX174, for which the DNA contribution near 830–840 cm^{-1} is calculable from the known tyrosine contribution as follows (Incardona et al., 1986).

The intensity of the tyrosine 644-cm^{-1} line (I_{644}) is not conformation sensitive, and the sum of intensities of the components of the tyrosine doublet ($I_{828} + I_{852}$) is independent of conformation even though the intensities of the individual Fermi components depend upon the hydrogen-bonding environment of the phenolic OH group (Siamwiza et al., 1975). Examination of Raman spectra of a large number of proteins of both viral and nonviral origins indicates that the quotient $R = (I_{644})/(I_{828} + I_{852})$ invariably falls within the narrow range 0.24 ± 0.018 (Verduin et al., 1984; Thomas, 1987; Li et al., 1990; and references therein). Values of R between 0.24 and 0.25 are especially well conserved among several mutants of the phage λ repressor DNA-binding domain (residues 1–102), even though the mutants differ greatly in the number and hydrogen-bonding environments of their tyrosines (Thomas et al., 1986b). Using the mean value for R of 0.24 ± 0.18,

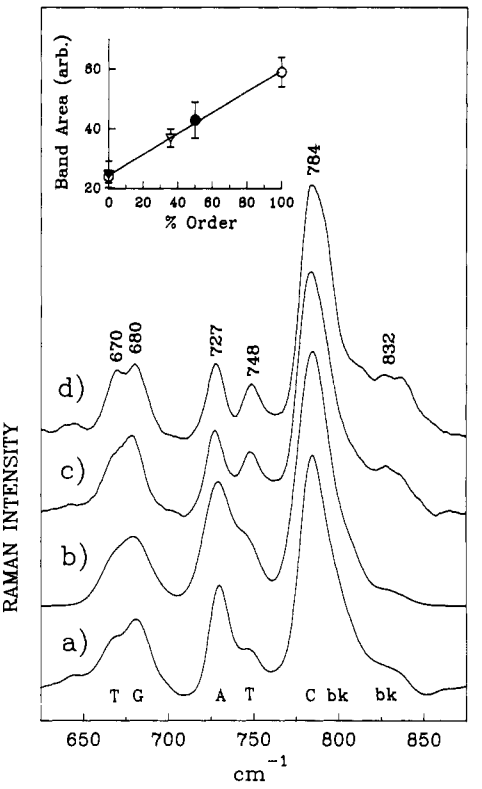

FIGURE 2: Comparison of Raman spectra in the region 600–900 cm^{-1} for DNAs containing different percentages of ordered (B-form) phosphodiester geometry. From bottom to top: (a) single-stranded O_L1+ at 55 °C (model for 0% order); (b) packaged ssDNA, obtained by Fourier deconvolution of data in Figure 1; (c) unpackaged ssDNA, from Figure 1; (d) double-stranded RFIII DNA at 12 °C (model for 100% order). The inset at upper left shows integrated 810–860-cm^{-1} Raman intensities of packaged (filled triangle) and unpackaged ssDNA (unfilled triangle) with respect to a calibration curve based upon (a) and (d) (unfilled circles). A data point (filled circle) for poly(rA)·poly(dT) (50% ordered B-form; see text) is included in the calibration curve.

together with the observed values of I_{644} and I_{852} from Figure 1, we calculate the expected tyrosine contribution at 828 cm^{-1} to be $I_{828} = (0.93 \pm 0.15)I_0$, where I_0 is the intensity actually observed at 828 cm^{-1} (arbitrary units, Figure 1). In other words, 93% of the Raman intensity at 828 cm^{-1} in the spectrum of Figure 1 is accounted for by tyrosine alone. The same result is obtained by use of band area in place of peak intensity measurement. The approximately 7% residual band intensity at 828 cm^{-1} represents the contribution from packaged ssDNA. The Raman profile of packaged ssDNA generated in this manner is compared with the spectrum of unpackaged (phenol-extracted) ssDNA in Figure 2. Conversion of this calculated result into a quantitative measure of packaged ssDNA secondary structure, with appropriate error limits, is illustrated in the inset of Figure 2 and described in more detail in section 3, below. We also describe in section 3 an alternative procedure for assessing the contribution of packaged ssDNA to the phage Raman spectrum ca. 830–840 cm^{-1}.

(2) Interpretation of Raman Marker Bands of ssDNA. The data of Figure 2 and Table I show that nucleosides of both packaged and unpackaged ssDNA exist predominantly as C2′-endo/anti conformers. On the other hand, the band near 830–840 cm^{-1}, which is diagnostic of B-type backbone geometry, is not present in the spectrum of packaged ssDNA. The absence of a significant DNA band near 830–840 cm^{-1} for the packaged DNA of ϕX174 was first reported by Incardona et al. (1987) and was interpreted as evidence of packaging-imposed constraint on the ssDNA secondary structure. To better

understand the nature of this constraint and to quantitate differences between secondary structures of packaged and unpackaged states of the ssDNA genome, we have developed the method described below for estimating the percentage of DNA nucleotides with phosphodiester torsions (α,ζ) configured as in the B-form (gauche$^-$,trans) of DNA.

(3) Percentage of B-Form Phosphodiester Geometry in ssDNA. (a) Determination by Compensation for Viral Proteins. Quantitative determination of ordered phosphodiester configurations in aqueous nucleic acids was first proposed for RNA on the basis of the observed direct proportionality between the intensity of the RNA band centered at 813 ± 1 cm^{-1} (Raman OPO symmetric stretching band) and the extent of ordered *A-type* (g$^-$,g$^-$) backbone geometry in RNAs of known secondary structure (Thomas, 1971; Lafleur et al., 1972; Brown et al., 1972). Applications to assess the degree of backbone order in tRNA, rRNA, and viral RNA have been described (Thomas & Hartman, 1973). Here, we propose a similar correlation between the Raman intensity of the B-form marker near 830–840 cm^{-1} and the extent of ordered *B-type* (g$^-$,t) backbone geometry. The present approach is complicated by the fact that the B-form marker exhibits a much broader spectral range than the corresponding A-form marker (Thomas et al., 1986a), viz., the former exhibits a range of peak frequencies between 830 and 840 cm^{-1} depending upon base composition and sequence, while the latter invariably occurs as a rather sharp band centered near 813 ± 1 cm^{-1}. Accordingly, the correlation proposed for DNA requires measurement of the integrated Raman band intensity extending from approximately 810 to 860 cm^{-1}, rather than measurement of the peak height of a single narrow band. As shown below, the band area measurement is facilitated by use of the Fourier deconvolution algorithm of Thomas and Agard (1984), which sharpens the band shape with conservation of the band area.

To relate the integrated intensity (810–860 cm^{-1}) of the backbone marker band to the percentage order in DNA, a minimum requirement is the corresponding Raman intensities for completely ordered and disordered models. To construct a simple calibration curve, we used the double-stranded RFIII DNA of φX174 as the completely ordered model (100% of OPO groups with B-type geometry, Figure 2d) and the single-stranded O_L1+ at 55 °C as the disordered model (Figure 2a). This calibration curve is shown in the inset to Figure 2. Our studies of O_L1+ indicate that hairpins are completely melted at 55 °C. [The Raman spectrum of O_L1+ displays no further diminution of intensity between 810 and 860 cm^{-1} at temperatures above 55 °C. The carbonyl region (1600–1700 cm^{-1}) of the D_2O solution Raman spectrum of O_L1+ also indicates no significant base pairing above 45 °C (G. J. Thomas, Jr., and J. M. Benevides, unpublished results).] As an additional data point on the calibration curve of Figure 2, we have included the appropriately normalized intensity of the 834-cm^{-1} Raman band in the heteronomous poly(rA)·poly(dT) structure (50% B-type geometry) which has been investigated recently (Benevides & Thomas, 1988).

To facilitate measurement of integrated intensities of backbone marker bands of Figure 2, we employed Fourier deconvolution as described previously (Thomas, 1985). The integrated intensities of the B-form marker bands (810–860 cm^{-1}) were normalized to the integrated intensity of the 680-cm^{-1} band of dG, which is the least affected by possible changes in base stacking and backbone geometry as long as the C2′-endo/anti dG conformation is conserved (Nishimura & Tsuboi, 1986; Benevides et al., 1988). Finally, we corrected

Table II: Raman Band Areas (650–875 cm^{-1}) for Backbone Conformation Analysis

σ	assignment[a]	ss O_L1+ 55 °C	φX174 dsDNA	φX174 unpackaged	φX174 packaged
665	T	18	21	14	17
682	G	29	25	26	26
730	A	44	30	30	42
750	T	15	21	22	20
782	C	100	98	94	89
792	bk	ND	36	20	10
800–804	bk	26	ND	7	
810–860	bk	24	59	37	23

[a] From Prescott et al. (1984) and references cited therein. A = adenine, C = cytosine, T = thymine, G = guanine, bk = backbone, ND = not detected. Band areas have been corrected for differences in base composition and are normalized with respect to the area of the 680-cm^{-1} band of guanine. Areas are given on an arbitrary 0–100 scale, with 100 assigned to the 782-cm^{-1} band of C.

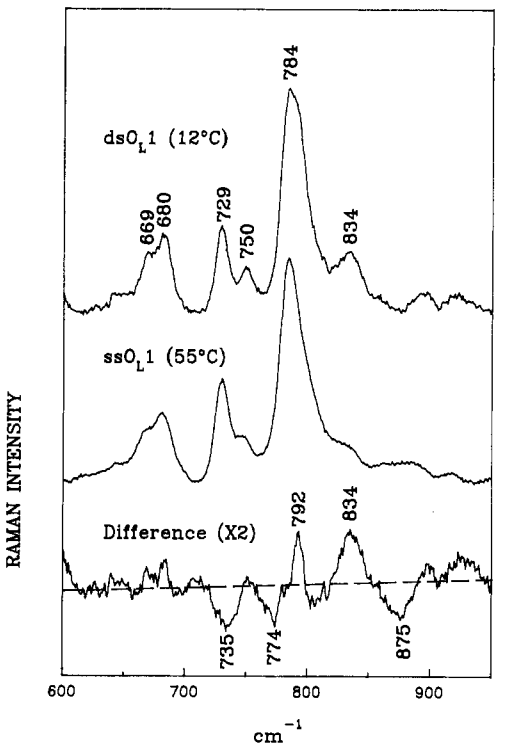

FIGURE 3: Raman spectra in the region 600–900 cm^{-1} of ds O_L1 at 12 °C (top), ss O_L1+ at 55 °C (middle), and their difference spectrum (bottom). Labels indicate difference bands which are discussed in the text.

the data for small differences in base composition of O_L1+, φX174 ssDNA, and φX174 dsDNA. Tabulation of the integrated and normalized band areas for the B-form marker bands and for other conformation-sensitive bands of the 600–900-cm^{-1} interval are given in Table II. The assignments for these bands have been discussed in detail elsewhere (Lord & Thomas, 1967; Erfurth & Peticolas, 1975; Prescott et al., 1984; Thomas et al., 1986a; Benevides et al., 1988; Thomas & Wang, 1988).

Table II shows that a discrete Raman marker band indicating the B-form phosphodiester geometry (g$^-$,t), is present in unpackaged but not in packaged ssDNA. The observed intensity corresponds to 36 ± 7% B-form nucleotide conformers in unpackaged ssDNA. Table II suggests further that the 792-cm^{-1} band intensity is closely correlated with that of the B-form marker and that as the intensities of the 792- and 834-cm^{-1} bands diminish, the underlying intensity near 875 cm^{-1} increases. This is clearly revealed in the spectral dif-

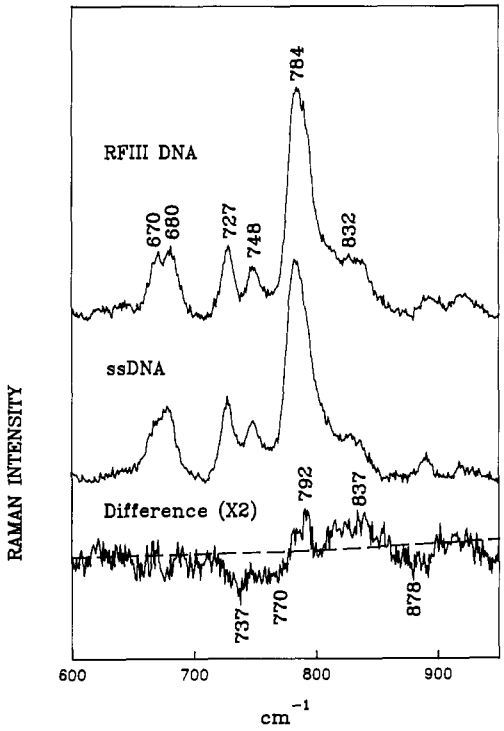

FIGURE 4: Raman spectra in the region 600–900 cm^{-1} of RFIII DNA (top), unpackaged ssDNA (middle), and their difference spectrum (bottom). Data were obtained at 12 °C.

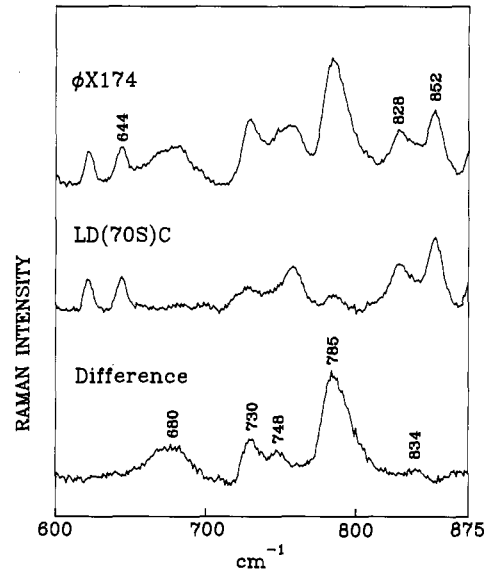

FIGURE 5: Raman spectra in the region 600–875 cm^{-1} of the ϕX174 virion (top), low-density 70S component (middle), and their difference spectrum (bottom). The important tyrosine and DNA bands discussed in the text are labeled in the top and bottom spectra, respectively. Spectral subtraction was normalized to the phenylalanine band at 622 cm^{-1}.

ferences between double-stranded O_L1 (12 °C) and single-stranded O_L1+ (55 °C), as shown in Figure 3. It is also evident in the comparison of RFIII dsDNA with unpackaged ssDNA shown in Figure 4. The overlap of the 792-cm^{-1} band with the intense cytosine band near 782 cm^{-1}, however, renders measurement of its integrated intensity impractical and disfavors its use in quantitative analyses.

Table II also shows that the intensity of the 730-cm^{-1} band of dA varies greatly with secondary structure, consistent with its demonstrated Raman hypochromicity (Tomlinson & Peticolas, 1970). Further discussion of this band is given in section 4, which follows. Relatively large intensity changes are also observed in bands of dT at 665 and 750 cm^{-1}, again consistent with data on model compounds (Thomas & Benevides, 1985). However, the dT band intensities are more difficult to interpret because of extensive overlap with neighboring bands (Figure 2).

The calibration curve proposed in the Figure 2 inset is based upon the assumption of linearity between the integrated 810–860-cm^{-1} intensity and the degree of ordered B-form structure. This assumption is supported by the fact that Raman band intensities generally exhibit linear dependence upon molecular concentration in solution phases, as well as by the localized nature of the OPO vibration. A similar linear relationship holds for the 813 ± 1 cm^{-1} band of RNA (Thomas & Hartman, 1973). To place error limits on the data points of the Figure 2 inset, we have employed the calculated ϕX174 DNA error limits from section 1 above and estimated the uncertainties associated with smoothing and selection of deconvolution parameters for the other data points. For example, in the case of dsDNA, smoothing of spectral noise leads to elimination of uncertainties of the order ±2% of the total band area, and varying the half-widths of deblurring functions by ±4 cm^{-1} changes the area of the resolved band by about ±5%.

In support of the determination described above, we have isolated for Raman spectroscopy a low-density fraction of DNA-deficient ϕX174 capsids. These particles, termed the "low-density 70S component", are shown by UV absorption spectroscopy, as well as by Raman spectroscopy, to lack at least 85% of the viral genome (unpublished data and Figure 5). X-ray crystallography indicates the same capsid morphologies for both native virions and the low-density particles (Willingmann et al., 1990). Therefore, we have obtained the Raman spectrum of the low-density 70S component as an approximation to a DNA-free ϕX174 capsid. Subtraction of the spectrum of the low-density 70S component from that of the native virion is expected to provide a good approximation to the Raman signature of the packaged viral genome. The results are shown in Figure 5.

The difference spectrum of Figure 5 shows clearly that the packaged ϕX174 genome lacks the prominent 834-cm^{-1} band of unpackaged ssDNA and exhibits only the feeble intensity which was obtained by the deconvolution procedure of section 1, above. The very weak 834-cm^{-1} band of the packaged ϕX174 genome is again shown to be consistent with that of the melted single-stranded model, O_L1+ (cf. Figure 2a,b with Figure 5, bottom). Thus, the spectral signature of the vast majority of ssDNA depleted from the native virion is that of "melted" ssDNA, i.e., DNA lacking the ordered B-form backbone. We note that the data of Figure 5 are also consistent with invariance of the tyrosine doublet intensity ratio to removal of packaged DNA.

(4) Estimation of Base Stacking in ssDNA. Raman bands of certain in-plane ring vibrations exhibit decreased intensity with stacking of the DNA bases, a phenomenon referred to as Raman hypochromism (Tomlinson & Peticolas, 1970). Table III lists Raman intensities for several DNA bands of the 600–1400-cm^{-1} interval assigned to in-plane ring vibrations of the bases (Lord & Thomas, 1967; Erfurth & Peticolas, 1975). Intensities in Table III were normalized to the 1090-cm^{-1} band (phosphodioxy symmetric stretch), which is not sensitive to base stacking or temperature.

Table III indicates that the most hypochromic bands are at 730 (dA), 1240 (dT + dC), and 1303 (dA) cm^{-1}. Assuming unit band intensities (i.e., no base stacking) in calf thymus DNA at 98 °C and maximal stacking at 25 °C, the data of Table III indicate near-maximal stacking in RFIII DNA at

Table III: Raman Band Areas for Analysis of Base Stacking[a]

band (cm^{-1})	assignment	CT DNA (25 °C)	CT DNA (98 °C)	change (%)	φX174 dsDNA	φX174 ssDNA	change (%)
680	G	0.41	0.43	+5	0.43	0.43	0
729	A	0.44	0.81	+84	0.43	0.52	+21
1240	T, C	0.50	1.24	+148	0.50	0.75	+50
1303	A	0.62	0.93	+50	0.60	0.69	+15
1340	A	0.88	1.01	+15	0.85	0.83	−2
1378	T	1.03	1.18	+15	1.00	1.02	+2

[a] Abbreviations: CT = calf thymus. Data for CT DNA are from Erfurth and Peticolas (1975) and Prescott et al. (1984); other data are from this work.

12 °C, and about 70% of maximal stacking in the unpackaged ssDNA molecule at 12 °C. Although similar analysis is not feasible for most Raman bands of packaged ssDNA due to interference from bands of the protein, the 730-cm^{-1} band is sufficiently well resolved (Figure 5) to indicate only a fraction of the hypochromism of unpackaged ssDNA, viz., about 40% of maximal base stacking. This indicates that in the packaged genome, at 12 °C, there is greatly reduced stacking of dA residues. By extension, we presume reduced stacking of other base residues of packaged ssDNA.

Discussion and Conclusions

In this work we have demonstrated directly that ordered deoxyribosyl phosphate groups of the B-type (g^-,t) geometry are present in φX174 ssDNA only when the molecule is removed (unpackaged) from the virion. When unpackaged, the ssDNA from φX174 contains 36 ± 7% of its nucleotides with the B-type backbone geometry. On the other hand, in the packaged state, φX174 ssDNA lacks ordered deoxyribosyl phosphate groups of the B-type geometry. The present findings refine earlier semiquantitative estimates by showing that residual Raman intensity at the position of the B-type marker band (810–860 cm^{-1}) is detected in single-stranded oligodeoxynucleotides at experimental conditions incapable of supporting helical hairpin formation. With this refinement we are able to conclude that *packaged ssDNA of φX174 contains essentially no ordered backbone geometry of the type prevalent in B-DNA, even though 36% of the residues of the unpackaged genome exhibit B-form geometry*. Accordingly, helical hairpins are not present to a significant extent in packaged φX174 ssDNA.

Consistent with the conclusion of a hairpin-deficient backbone, we observed considerably less Raman hypochromism (≈40%) for packaged than for unpackaged (≈70%) ssDNA. We conclude that packaging the φX174 genome restricts both base pairing and base stacking.

A similar conclusion has been reached for packaged ssDNA of the filamentous phage fd, by using trioxalen cross-linking (Shen et al., 1979). A single, unique 170 bp hairpin region, located at the nonadsorbing end of the virion (Webster et al., 1981), was cross-linked when the reaction was carried out with intact phage. From this finding it was concluded that the remainder of the ssDNA interacts with the viral gene VIII capsid protein in such a way as to prevent formation of additional hairpin structures.

Hairpins are present in unpackaged, circular fd ssDNA, since a significant increase in the number of cross-linked regions is observed when the trioxalen procedure is applied to free ssDNA (Shen & Hearst, 1976). Furthermore, the amount of cross-linking is dependent on the ionic strength. At 15 °C and in TE buffer alone no hairpins are detected. With the addition of 30 mM NaCl most of the cross-linked ssDNA molecules exhibit four or five hairpins; and at 40 mM NaCl as many as eight total hairpins are observed. At 100 mM, the salt concentration used in the present study, collapsed treelike structures are observed in the electron micrographs, indicating extensive hairpin formation. Thus, packaging circular ssDNA in either a filamentous or icosahedral protein shell significantly reduces the number of bases involved in helical base-paired structures. In both phages this is presumably due to DNA–protein interactions.

However, the observation that packaged fd ssDNA has one hairpin (of 170 bp), while packaged φX174 ssDNA may not, could be biologically significant. Dotto and Zinder (1983) showed that the fd hairpin is a packaging signal for the assembly of mature virion filaments. More recent work by Russell and Model (1989) supports its site of action at the host membrane where the gene VIII coat protein is exchanged for the phage gene V DNA-binding protein. In the case of φX174 the synthesis of progeny ssDNA is coupled with packaging into an essentially spherical prohead (Aoyama et al., 1983). Thus, there may be no requirement for an analogous packaging signal in φX174 ssDNA. Furthermore, lack of hairpin structures is not simply a consequence of an icosahedral shell. As previously noted (Incardona et al., 1987), the isometric ssRNA plant and bacterial viruses have packaged genomes with 80–95% of their nucleotides in ordered conformations.

Although the present studies do not reveal the nature of local nucleotide interactions which prevent hairpin formation, two obvious possibilities are (i) binding to the capsid wall and (ii) binding to the basic gpJ protein which is presumably packaged along with ssDNA (Aoyama et al., 1983; Casjens, 1985). Specific icosahedral binding of a packaged viral genome has been observed in the crystal structure of bean pod mottle virus (Chen et al., 1989), and similar packaging has been inferred for the solution structure of BPMV (Li et al., 1990). However, only 15–20% of the packaged BPMV RNA can be accounted for in the electron density map; and, interestingly, RNA–capsid coordination occurs with essentially complete conservation of the A-type (g^-,g^-) ribosyl phosphate backbone geometry (Li et al., 1990). Therefore, icosahedrally symmetric coordination of ssDNA with the φX174 capsid is unlikely to account fully, if at all, for the absence of an oriented DNA backbone. Conformational constraints imposed by packaging would appear to result principally from interaction of ssDNA with the 60 gpJ subunits. Assuming stoichiometric binding, we expect ≈90 nucleotides coordinated per gpJ subunit and/or capsid heterodimer (gpF + gpG). Further studies are planned to investigate directly the DNA binding affinities of gpJ and the capsid heterodimer.

With regard to our results on unpackaged φX174 ssDNA, we note the following. The stability of nucleic acid hairpins in solutions of moderate ionic strength has been well established from numerous studies of ssRNA (Jacobsen, 1976). RNA hairpins with ordered (A-type) backbones may incorporate as many as 60% of ribonucleotides as paired bases (Wells et al., 1980). Since hairpin formation is clearly favored for ssRNA, hairpins might also have been expected for ssDNA

at the conditions of our experiments. Indeed, application of an RNA energy minimization algorithm to ϕX174 ssDNA predicts a highly folded structure with extensive intramolecular base pairing (Nussinov & Piecznik, 1984). Yet, only 36% of the nucleotides in the circular ϕX174 ssDNA are in the B-type backbone conformation. In the case of viral ssRNA there is closer agreement between secondary structure predictions and experimental findings.

One obvious difference between ssRNA and ssDNA is the circular covalency of the latter. However, this is probably not sufficient to constrain the secondary structure for the following reasons. First, Shen and Hearst (1976) obtained essentially the same number and distribution of hairpins for the linearized form of fd genomic ssDNA as they found with circular fd ssDNA. Second, Edlind and Ihler (1980) compared long-range base pairing in linear and circular ϕX174 ssDNA and found that the number, size, and location of loops were essentially the same for the two forms, although the frequency of small loop formation may have been higher in linear molecules. Third, a direct comparison of the resistance of the two phage DNAs to single-strand-specific nucleases (as a measure of double-strand formation) reveals that both ϕX174 and fd circular forms contain only 2–3% of their bases in such structures (Bartok et al., 1975; Schaller et al., 1969). By this criterion the two DNAs appear to have similar secondary structures throughout their entire sequences. Thus, circularization is unlikely to account for the low level of secondary structure observed in unpackaged ϕX174 ssDNA.

The use of vibrational spectroscopy to quantitatively assess nucleic acid secondary structure has been demonstrated in both infrared (Thomas, 1969) and Raman applications to ssRNA (Thomas, 1971; Thomas & Hartman, 1973). The present study extends the Raman method to ssDNA and demonstrates for the first time in quantitative terms a difference in the degree of order between protein-free and protein-packaged states of the same viral DNA molecule. The Raman method has the advantages of being quantitative, highly sensitive, free of chemical artifacts, and applicable to base-paired stems of any length.

Acknowledgments

We thank Ms. Stacy Towse and Ms. Kelly Aubrey (UMKC) for assistance in sample handling and data collection and Dr. Gopal Murti and Kathy Troughton of St. Jude Children's Research Hospital, Memphis, for the electron microscopy.

References

Aoyama, A., Hamatake, M., & Hayashi, M. (1983) *Proc. Natl. Acad. Sci. U.S.A. 80*, 4195–4199.

Bartok, K., Harbers, B., & Denhardt, D. T. (1975) *J. Mol. Biol. 99*, 93–105.

Benevides, J. M., & Thomas, G. J., Jr. (1988) *Biochemistry 27*, 3868–3873.

Benevides, J. M., Wang, A. H.-J., van der Marel, G. A., van Boom, J. H., Rich, A., & Thomas, G. J., Jr. (1984) *Nucleic Acids Res. 12*, 5913–5925.

Benevides, J. M., Wang, A. H.-J., Rich, A., Kyogoku, Y., van der Marel, G. A., van Boom, J. H., & Thomas, G. J., Jr. (1986) *Biochemistry 25*, 41–50.

Benevides, J. M., Wang, A. H.-J., van der Marel, G. A., van Boom, J. H., & Thomas, G. J., Jr. (1988) *Biochemistry 27*, 931–938.

Birnboim, H. C., & Doly, J. (1979) *Nucleic Acids Res. 7*, 1513–1518.

Brown, K. G., Kiser, E. J., & Peticolas, W. L. (1972) *Biopolymers 11*, 1855–1869.

Burgess, A. B. (1969) *Proc. Natl. Acad. Sci. U.S.A. 64*, 613–617.

Casjens, S. (1985) in *Virus Structure and Assembly* (Casjens, S., Ed.) pp 75–147, Jones & Bartlett, Boston.

Chen, Z., Stauffacher, C., Yunge, L., Schmidt, T., Bomu, W., Kamer, G., Shanks, M., Lomonossoff, G., & Johnson, J. E. (1989) *Science 245*, 154–159.

Dotto, G. P., & Zinder, N. D. (1983) *Virology 130*, 252–256.

Edlind, T. D., & Ihler, G. M. (1980) *J. Mol. Biol. 142*, 131–144.

Erfurth, S. C., & Peticolas, W. L. (1975) *Biopolymers 14*, 247–264.

Erfurth, S. C., Kiser, E. J., & Peticolas, W. L. (1972) *Proc. Natl. Acad. Sci. U.S.A. 69*, 938–941.

Hayashi, M., Aoyama, A., Richardson, D., Jr., & Hayashi, M. N. (1988) in *The Bacteriophages* (Calendar, R. Ed.) Vol. 2, pp 1–71, Plenum Press, New York.

Incardona, N. L., Tuech, J. K., & Murti, G. (1985) *Biochemistry 24*, 6439–6446.

Incardona, N. L., Prescott, B., Sargent, D., Lamba, O. P., & Thomas, G. J., Jr. (1987) *Biochemistry 26*, 1532–1538.

Jacobson, A. B. (1976) *Proc. Natl. Acad Sci. U.S.A. 73*, 307–311.

Kornberg, A. (1980) *DNA Replication*, Freeman, San Francisco.

Lafleur, L., Rice, J., & Thomas, G. J., Jr. (1972) *Biopolymers 11*, 2423–2437.

Li, T., Chen, Z., Johnson, J. E., & Thomas, G. J., Jr. (1990) *Biochemistry 29*, 5018–5026.

Lord, R. C., & Thomas, G. J., Jr. (1967) *Spectrochim. Acta 23A*, 2551–2591.

Nishimura, Y., & Tsuboi, M. (1986) in *Spectroscopy of Biological Systems* (Clark, R. J. H., & Hester, R. E., Eds.) Advances in Spectroscopy, Vol. 13, pp 177–232, Wiley, New York.

Nussinov, R., & Piecznik, G. (1984) *J. Theor. Biol. 106*, 261–273.

Prescott, B., Steinmetz, W., & Thomas, G. J., Jr. (1984) *Biopolymers 23*, 235–256.

Russell, M., & Model, P. (1989) *J. Virol. 63*, 3284–3295.

Sanger, F., Coulson, A. R., Freidmann, T., Air, G. M., Barrell, B. G., Brown, N. L., Fiddes, J. C., Hutchison, C. A., III, Slocombe, P. M., & Smith, M. (1978) *J. Mol. Biol. 125*, 225–246.

Schaller, H., Voss, H., & Gucker, S. (1969) *J. Mol. Biol. 44*, 445–458.

Shaw, D. C., Walker, J. E., Northrop, F. D., Barrell, B. G., Godsen, G. N., & Fiddes, J. C. (1978) *Nature 272*, 510–515.

Shen, C.-K. J., & Hearst, J. E. (1976) *Proc. Natl. Acad. Sci. U.S.A. 73*, 2649–2653.

Shen, C.-K. J., Ikoku, A., & Hearst, J. E. (1979) *J. Mol. Biol. 127*, 163–175.

Siamwiza, M. N., Lord, R. C., Chen, M. C., Takamatsu, T., Harada, I., Matsuura, H., & Shimanouchi, T. (1975) *Biochemistry 14*, 4870–4876.

Siden, E. J., & Hayashi, M. (1974) *J. Mol. Biol. 89*, 1–16.

Thamann, T. J., Lord, R. C., Wang, A. H.-J., & Rich, A. (1981) *Nucleic Acids Res. 9*, 5443–5457.

Thomas, G. J., Jr. (1969) *Biopolymers 7*, 325–334.

Thomas, G. J., Jr. (1971) in *Proceedings, Spectrum of Light Scattered from Biological Molecules*, MIT, Cambridge, MA.

Thomas, G. J., Jr. (1985) *Spectrochim. Acta 41A*, 217-221.
Thomas, G. J., Jr. (1987) in *Biological Applications of Raman Spectroscopy* (Spiro, T. G., Ed.) Vol. 1, pp 135-201, Wiley, New York.
Thomas, G. J., Jr., & Hartman, K. A. (1973) *Biochim. Biophys. Acta 312*, 311-322.
Thomas, G. J., Jr., & Agard, D. A. (1984) *Biophys. J. 46*, 763-768.
Thomas, G. J., Jr., & Benevides, J. M. (1985) *Biopolymers 24*, 1101-1105.
Thomas, G. J., Jr., & Wang, A. H.-J. (1988) in *Nucleic Acids and Molecular Biology* (Eckstein, F., & Lilley, D. M. J., Eds.) Vol. 2, pp 1-30, Springer-Verlag, Berlin.
Thomas, G. J., Jr., Li, Y., Fuller, M. T., & King, J. (1982) *Biochemistry 21*, 3866-3878.
Thomas, G. J., Jr., Benevides, J. M., & Prescott, B. (1986a) *Biomol. Stereodyn. 4*, 227-254.
Thomas, G. J., Jr., Prescott, B., Benevides, J. M., & Weiss, M. A. (1986b) *Biochemistry 25*, 6768-6778.
Tomlinson, B. L., & Peticolas, W. L. (1970) *J. Chem. Phys. 52*, 2154-2156.
Verduin, B. J. M., Prescott, B., & Thomas, G. J., Jr. (1984) *Biochemistry 23*, 4301-4308.
Webster, R. E., Grant, R. A., & Hamilton, L. A. W. (1981) *J. Mol. Biol. 152*, 357-374.
Wells, R. D., Goodman, T. C., Hillen, W., Horn, G. T., Klein, R. D., Larson, J. E., Muller, U. R., Neuendorf, S. K., Panayotatos, N., & Stirdivant, S. M. (1980) *Prog. Nucleic Acids Res. Mol. Biol. 24*, 167-267.
Willingmann, P., Krishnaswamy, S., McKenna, R., Smith, T. J., Olson, N. H., Rossmann, M. G., Stow, P. L., & Incardona, N. L. (1990) *J. Mol. Biol. 212*, 345-350.

Removal of DNA Curving by DNA Ligands: Gel Electrophoresis Study†

Francisca Barcelo,‡,§ Gabriel Muzard,‡,∥ Roberto Mendoza,‡ Bernard Rêvet,‡ Bernard Pierre Roques,⊥ and Jean-Bernard Le Pecq*,‡

Unitê de Physicochimie Macromolêculaire et Laboratoire de Microscopie Cellulaire et Molêculaire, INSERM U140, CNRS URA147, Institut Gustave-Roussy, 94805 Villejuif Cedex, France, and Dêpartement de Chimie Organique, INSERM U266, CNRS URA498, UER des Sciences Pharmaceutiques et Biologiques, 4 Avenue de l'Observatoire, 75006 Paris, France

Received November 7, 1990; Revised Manuscript Received February 8, 1991

ABSTRACT: The removal of inherent curving in *Crithidia fasciculata* kinetoplast DNA by various small DNA ligands, groove binders and mono- and bisintercalators, has been studied by gel retardation and electron microscopy. The migration of the kinetoplast DNA fragment is highly retarded during gel electrophoresis. We demonstrate that this retardation is suppressed by DNA ligands such as distamycin and ditercalinium, which have different modes of binding and sequence specificities. Observation by electron microscopy confirms that the effect of ditercalinium on gel migration of curved DNA is linked to DNA uncurving. As the drug is progressively added to DNA, a large broadening of the retarded band is observed during gel electrophoresis for distamycin and ditercalinium. In the case of distamycin, the retarded DNA band splits into two broad bands, whereas the noncurved DNA bands remain homogeneous. This indicates that the drug–DNA exchange is extremely slow in the gel and that a limited number of specific sites on DNA are critical for the removal of bending. GC-specific quinomycin, monointercalators, and bisintercalators act in a manner similar to that of AT-specific distamycin. This indicates that direct drug binding at the dA_n tracts is not required for DNA uncurving. We propose that the uncurving of kinetoplast DNA by drugs is caused by a global alteration of DNA structure; subsequent increased flexibility leads to the suppression of rigid bending at the AT tract junctions.

DNA sequences such as enhancers control the activity of promoters located at a distance on the DNA molecule. It has been shown that such remote control involves the interaction of proteins bound at distant sites on DNA through the formation of DNA loops. The implication of DNA looping in various biological processes has recently been discussed (Schleif, 1988). The formation of such DNA loops is limited by the bending ability of DNA (Wang & Giaever, 1988).

Therefore, inherently curved DNA sequences (Trifonov & Ulanovsky, 1988) would favor the interaction of proteins bound at distant sites on DNA by decreasing the free energy of loop formation. In this context, knowing whether small ligands such as antibiotics or antitumor drugs are able to remove or induce DNA curvature is of crucial importance.

Gel electrophoresis is a very powerful technique for the analysis of DNA bending. It demonstrated that pyrimidine dimers and covalent adducts such as GG intrastrand cisplatinum adducts induce DNA bending (Rice et al., 1988). On the other hand, the photoactivated covalent fixation of trimethylpsoralen on DNA was not found to produce significant bending (Sinden & Hagerman, 1984; Haran & Crothers, 1988).

Gel electrophoresis has also been used to analyze the effect of the reversible binding of proteins on DNA. No dissociation has been observed during gel migration because of the highly stable complexes. Therefore, the reversible complex could be analyzed in the same way as a covalent adduct. However, this method, which is appropriate for protein–DNA complexes, is not expected to be suitable for the study of the DNA bending induced by ligands that have a relatively small DNA binding

† This work was supported by INSERM, Contrat de Recherche 862009.
* To whom correspondence should be addressed.
‡ Institut Gustave-Roussy.
§ Present address: University les Iles Balears, Department of Biology, Faculty of Sciences, 07071 Palma of Mallorca, Spain.
∥ Present address: Laboratoire Theramex, BP 59, Monaco.
⊥ UER des Sciences Pharmaceutiques et Biologiques.

0006-2960/91/0430-4863$02.50/0 © 1991 American Chemical Society